Chapter 5

Silicon Avalanche Based Light Emitting Diodes and Their Potential Integration into CMOS and RF Integrated Circuit Technology

Kaikai Xu, Weifeng Sun, Kingsley A. Ogudo, Lukas W. Snyman, Jean-Luc Polleux, Qi Yu and Guannpyng Li

Additional information is available at the end of the chapter

http://dx.doi.org/10.5772/58968

1. Introduction

As a rapid growing field in worldwide science and technology, silicon nano-photonics has become one of the most promising photonics integration platforms in the last decade. This is mainly due to the combination of a very high index contrast and the availability of silicon complementary metal-oxide-semiconductor (CMOS) fabrication technology, which allows the use of electronics fabrication facilities to make photonic circuitry. Unfortunately, the indirect band-gap of silicon leads to low efficiency and slow efficiency that is unexpected. The rate of electron-hole recombination in silicon material is too low to produce emitted photons in forward biased silicon p-n junctions, but light emission observed from reverse-biased silicon p-n junctions under high electric field was already reported in 1955 by Newman [1]. The radiative transition between hot carriers emits photons larger than the energy gap. Hence the luminescence during avalanche breakdown is characterized by a broad emission spectrum. An example of the high-energy edges of avalanche-breakdown luminescence is shown in Fig. 1. The low-energy edge of the emission spectrum, on the other hand, extends to energies lower than the gap energy, due to the tunneling-assisted photon emission [2].

Since electron-hole pairs are produced during avalanche breakdown, some radiative recombination occurs. Both the electrons and the holes can be heated by the electric field. Since it is attributed to the hot-carrier population under the condition of avalanche breakdown, the light emission can be used for high-speed light-emitting devices, high-speed light amplifiers, and the analytic investigation of hot carrier distribution [3].

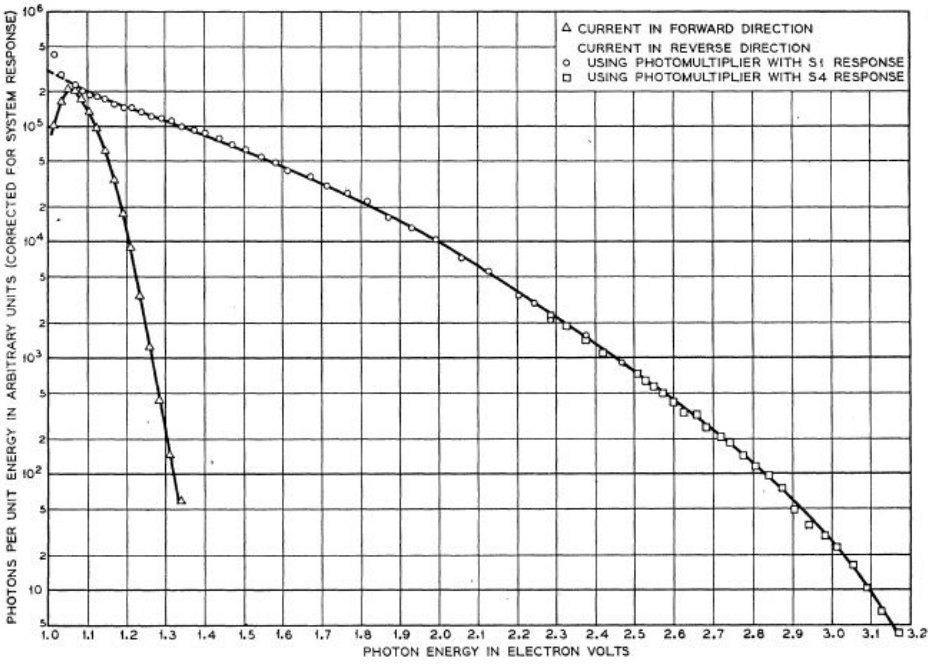

Figure 1. The emission spectra for both forward and breakdown currents corrected for the spectral response of the spectrometer-photomultiplier system (After ref. [2]).

Conventional electric interconnection in today's computers has been a bottleneck for high-speed and large-capacity data transmission. To break through this bottleneck, substituting electric interconnection by optical interconnection is a possible direction [4].

Ideally, all three components (i.e., light source, waveguide, and photo-receiver) of the optical link should be monolithically integrated with the silicon substrate chip and be compatible with complementary metal-oxide semiconductor (CMOS) technology. Silicon photo-receiver circuits can be readily embedded in silicon chips, and silicon-on-insulator (SOI) optical waveguides (i.e., SiO_2 layer) may be used as optical connections. The main difficulty lies in transmitters since light sources can not be efficiently made with silicon because it is an indirect-bandgap material. Efficient light-emitting materials, such as AlGaAs/GaAs, grown on silicon substrates by heteroepitaxy are not sufficiently reliable because of the lattice-parameter and thermal-expansion mismatch between the two materials. One practical approach to addressing the mismatch between the compound-semiconductor optoelectronic technology which is used to fabricate optical sources, and the CMOS silicon technology which is the basis of modern electronics, is the hybrid integration. This approach is based on bonding separately fabricated optoelectronic and electronic chips. A hybrid-integration process known as flip-chip bonding can integrate thousands of optoelectronic devices on a single silicon chip with lateral alignment better than 1 micron [5].

http://dx.doi.org/10.5772/58968

Despite the indirect band-gap, one of the most promising candidate light sources is now thought to be silicon itself because LEDs made of silicon-based materials can be integrated into the existing microelectronic and optoelectronic technologies in a highly economic way. The ideas for direct generation (i.e., electron-hole recombination) of light in silicon by the use of photonic-crystal structure remain in the domain of ongoing research, since the spatial confinement of electron-hole pair on silicon nano-crystal separated by a high-barrier oxide is able to reduce the non-radiative recombination probability and increase the luminescence. Several approaches, such as porous silicon [6, 7], silicon-silicon dioxide superlattice [8], silicon nanoparticles in silicon dioxide [9], erbium in silicon [10–12], silicon/germanium [13–17], and iron disilicide [18], have been considered to enhance its poor light emission. However, these approaches are too complicated to be perfectly compatible with the standard CMOS process technology.

In the present chapter, we will give an overview of the field-effect electroluminescence in the reverse-biased silicon p-n junctions. The following is an outline of the topics covered here. Section 2 provides the construction of a theoretical model which includes the intraband transition and the interband transition of silicon reverse-biased p-n junction electro-optical properties. Section 3 expands the analysis to the explore the silicon gate-controlled diode (a reverse-biased p-n junction with the an additional terminal) that might influence silicon LED: this will indeed show that the, in contrast to the two-terminal Si-diode LED, the three-terminal Si gate-controlled diode LED is able to control the light intensity by adjusting the gate voltage V_g. Since the N^+drain to P^+substrate junction in an N-channel MOSFET (N-MOSFET) device is also a reverse-biased p-n junction, the phenomenon of light emission from the silicon metal-oxide-semiconductor field-effect-transistor (Si-MOSFET) operating in the saturation mode is analyzed by a novel model of physical mechanism in Section 4. Section 5 and 6 present the substantial input in realizing the optical link structures. Finally, Section 7 concludes that the silicon LED will significantly play an important role in future silicon photonic-electronic-integrated-circuits (PEICs).

2. Silicon CMOS avalanche LED

Silicon the material per excellence for electronics is not used for sourcing light due to the lack of efficient light emitter and lasers. In general, high-field electroluminescence can be divided into three categories [19],

- Electroluminescence of powder phosphors (the original discovery by Destriau falls into this category– the phosphor particles were dispersed in a dielectric)
- Electroluminescence of thin films (a homogeneous thin layer of a phosphor filing up the space between capacitor plates-electrodes)
- Electroluminescence of a reverse-biased p-n junction.

In this section, photon emission from silicon was observed by using a p-n junction that operates in the reverse breakdown mode. Indeed, a PMOSFET device can works two p-n junction

diodes, as shown in Fig. 2, if both the p⁺drain and p⁺source are grounded while the gate is floated. Substrate voltage V_{sub} is defined as the reverse bias of the two in-parallel connected p-n junction diodes.

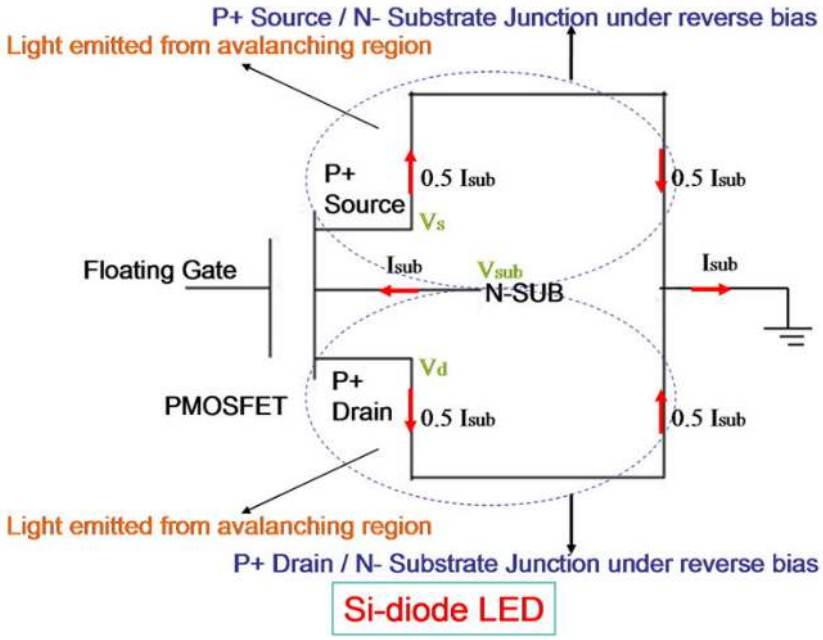

Figure 2. Schematic presentation of the Si-PMOSFET device for the case of Si-diode LED.

In Fig. 3 it is discovered that this radiation originates first in the isolated spots in the close vicinity of the junction area, and with increasing reverse bias these spots merge into a single homogeneous emitting area.

The explanation of this effect is based on the close link between electroluminescence and the electrical breakdown of a reverse-biased p-n junction, as depicted in Fig. 4. At reverse bias, the injection of electrons from n region to the p region and of holes from the p region to the n region can not be achieved. The saturation current across the junction arises from thermally generated minority carriers on both sides of the junction. Due to the high-field, an electron or hole ionizes the lattice, a free *e-h* pair is created and an avalanche like increase in the number of free carriers evolves. The current is increasing substantially, and electron-hole pairs with substantial excess energy gained by the acceleration can, naturally, recombine radiatively.

In addition to Fig. 2, Fig. 5 shows one-half of a PMOSFET-like device that can work as the reverse-biased p-n junction. The device is fabricated using the standard 3μm CMOS process with self-aligned technology. The shape of the spectra and the peaks of emission are basically

http://dx.doi.org/10.5772/58968

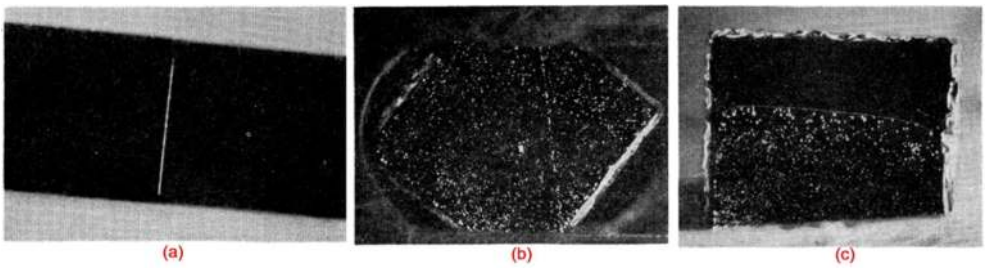

Figure 3. The dark field optical micrograph of the visible light from the reverse-biased silicon p-n junction: (a) The light emission from a grown junction interprets the surface; (b) The light emission pattern from a junction diffused to a depth of a bout 2 microns below the crystal surface, as see in the direction normal to the surface; (c) The light emission from a junction similar to that of (b) except that part of the surface has been ground off at an angle of one degree to the remainder. The sharp white line marking the boundary of the light spots indicates where the junction intercepts the sloping face. (After ref. [2]).

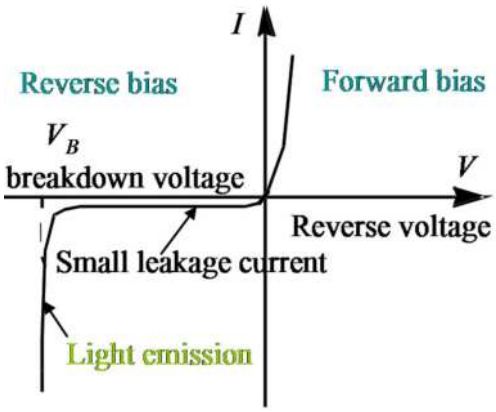

Figure 4. The current-voltage characteristic of a reverse-biased p-n junction.

unchanged under different reverse-bias conditions. Two distinguished wavelength peaks are observed to occur at 650 nm and 750 nm, as shown in Fig. 6.

Normally, in the microplasma (the prerequisite for the assumption of Braking radiation) or avalanche region of the reverse-biased p-n junction, both the holes and hot electrons are presented up to 2.4 eV (corresponding to wavelength ~550 nm) of the pair production threshold for holes and 1.8 eV (corresponding to wavelength ~650 nm) of the pair production threshold for electrons due to high accelerating field [21]. On the other hand, the accelerated carriers will lose some kinetic energies through the collision with artifical atoms (i.e., immobile charged centers) in the depletion region of p-n junction, and the lost energies will be released in the form of photons. On the origin of Bremsstrahlung radiation mentioned previously, the primary wavelength peak 650 nm and the subsidiary wavelength peak 550 nm may be explained by the two threshold values. In fact, the mechanism behind the light emission under the avalanche

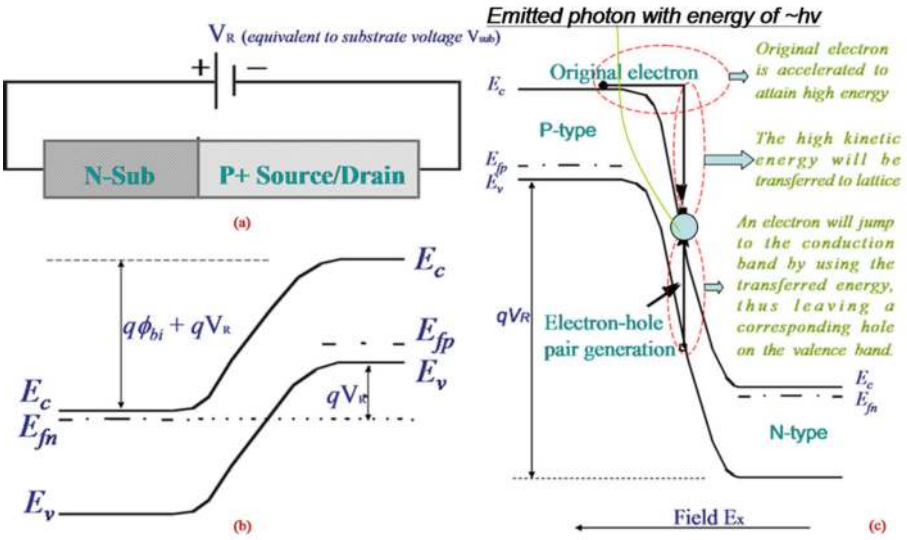

Figure 5. Energy band scheme which demonstrates current amplification due to impact ionization and depicts radiative recombination of an *e-h* pair giving.

breakdown condition is extremely complicated, and there are other possible mechanisms contributing to this type of light emission besides Bremsstrahlung radiation. In [22], a reasonable model is proposed to indicate that avalanche emission in silicon longer than ~620 nm is primarily due to indirect interband transition by high-field carrier populations, that Bremsstrahlung (i.e., indirect intraband transition) dominates the range of ~539 nm to ~620 nm, and that direct intraband transition should be the main reason for the photon emission with wavelength shorter than ~539 nm. Accordingly, it is suggested that the overall mechanism is too complicated to be explained by Bremsstrahlung only. The influence of the defects on the localized emitting spots also should be taken into consideration. In addition, the interference of the emitted light by the passivation layer on the surface of the silicon substrate may account for some of the light intensity sub-crests exhibited in Fig. 6.

The visible light emitted from silicon p-n junction reverse-biased at high voltages has been studied and analyzed. This hot-electron electroluminescence has been seen to offer a useful mean for the study of high-field effects, device integrity, transport, real-space transfer and electron energy distributions. Examination of the electroluminescence distribution reveals the electrical weak spots of the silicon device and may indicate the presence of localized breakdown. Spectral measurements suggest that a number of mechanisms contribute to the visible light emission, including indirect intraband transitions and band-band recombination. Lacaita *et al.* explained that the light emission processes in avalanching reverse-biased p-n junctions should be due to electron and hole relaxation and recombination processes occurring in the high-field avalanching region in theory [23]. In contrast, from experimental evidence and models, Bude *et al.* concluded that intraband electron relaxation processes of electrons

http://dx.doi.org/10.5772/58968

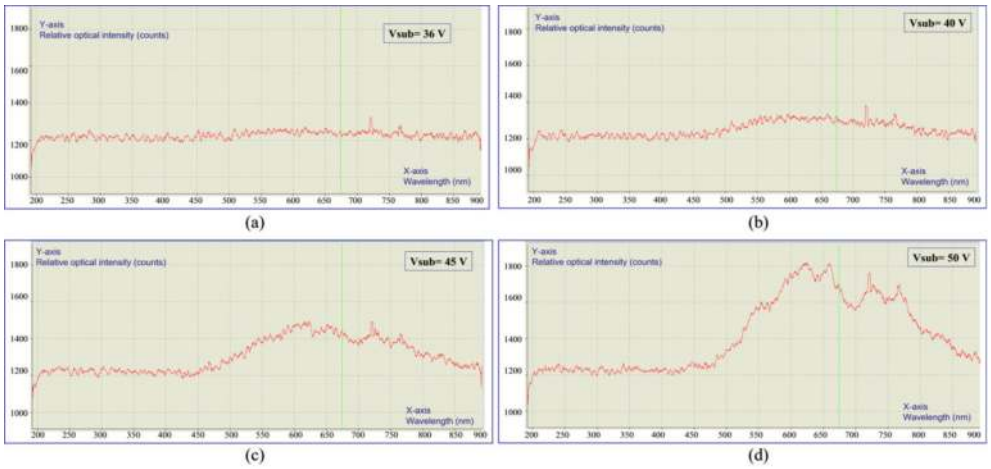

Figure 6. Output emission spectra of the Si light-emitting-device, gate is floated, V_s=V_d=0 V. Emitting wavelength ranges from 500 nm to 850 nm in the measured range of 200 nm to 900 nm (After ref. [20]).

occurring within the conduction band of the silicon itself should be the major reason [24]. It should be noted that a detailed study of the spectrum further allows analysis of the carrier distribution, scattering direction and conduction electron temperature in the space-charge region of silicon p-n junctions.

Commonly, the mechanism of this optical radiation could be explained by the classical electromagnetic theory in which an electron collides with a singly charged Coulombic center. Furthermore, the phenomenon and the rate expression of continuous x-ray spectrum (i.e., Bremsstrahlung radiation) are able to interpret the optical emission observed in the reverse-biased silicon diode if the space-charge region is approximately treated as micro-plasma. It is noted that the x-ray scattering process is distinguished from optical scattering because the energy of the incident x-ray photon with frequency ν_0 becomes large enough with respect to the rest energy of the electrons to give a significant frequency shift to the scattered radiation [25]. In fact, the incident carriers generated by impact ionization will be accelerated by the high field in order to collide with the Coulombic charged centers (i.e., artificial atoms [26]), and then the loss of kinetic energy will be released in the form of photons. The ratio of the Coulombic interaction energy to the thermal energy is given by

$$\Gamma_e = \frac{1}{4\pi\varepsilon_{si}} \frac{q^2}{rkT_e} \tag{1}$$

where k is the Boltzmann constant, T_e is the effective temperature, ε_{si} is the dielectric constant of silicon, and q is the magnitude of elementary charge. r, which is defined as the inter-particle spacing (i.e., Wigner-Seitz radius), is

$$r = \left(\frac{3}{4\pi n} \right)^{1/3} \tag{2}$$

where n denotes the ion density. In accordance with the theory of "hot carrier", the condition for full ionization usually means that the thermal energy of the particles exceeds the ionization energy of the atoms from which the plasma is formed

$$E_{thermal} = \frac{3}{2} kT_e > E_{ion} \tag{3}$$

In addition, the lifetime of the excited state is expressed as [27]

$$\tau = \frac{h}{kT_e} \tag{4}$$

where h is the Planck constant. Since Coulomb collisions serve for distribution of the reduced velocity of carrier, the variation of velocity is usually written as

$$\Delta v = \frac{hK}{m} \tag{5}$$

where K is the photons wave number and m is the ions mass.

The motion of thermal carriers resembles that of a dilute gas, and the distribution of the kinetic energy of thermal carriers can be described by the Maxwell-Boltzmann distribution, derived from the kinetic theory of gases. The probability of carriers having an energy E is expressed in the form

$$\frac{n(E)dE}{n} = \frac{2\pi\sqrt{E}}{\left(\sqrt{\pi kT_e}\right)^3} \exp\left(-\frac{E}{kT_e} \right) dE \tag{6}$$

where $n(E)dE$ is the number of carriers of energy from E to $E + dE$, n is the total number of carriers in the space-charge region which approximately is gas-microplasma, k is the Boltzmann constant, and T_e is the absolute temperature. This distribution gives an energy corresponding to the most probable velocity, or 0.025 eV at 300 K. The temperature, T_e, associated with a Maxwell's distribution of a carrier population, is also called the "carrier temperature".

Using Maxwell's equation in which the particles are the sources for current and charge distribution, the exact field at the position of the particle can be obtained from self-consistent calculation. Consequently, the kinetic equation becomes

http://dx.doi.org/10.5772/58968

$$\frac{\partial f_\alpha}{\partial t} + \vec{v} \bullet \nabla f_\infty + \frac{q}{m}\left(\vec{\mathrm{E}} + \vec{v} \times \vec{\mathrm{B}}\right) \bullet \nabla_v f_\alpha = \left(\frac{\partial f_\alpha}{\partial t}\right)_{coll} \tag{7}$$

where the left hand side contains only averaged quantities and the so-called collision terms on the right hand side contains all microscopic interactions [28]. In general, the existence of radiative elastic collisions (*Bremsstrahlung*) is the scattering of an electron by an external field, accompanied by the emission of a photon. Considering charge-charge or charge-neutral elastic collisions, the collision frequency is calculated as follows. The collision time $\tau = \frac{1}{\nu}$ is the time for a charge to experience a significant deflection (i.e., change in momentum). The equation of conversion of momentum for the species α is obtained by multiplying Eq. (7) by mv_α and then integrating over v_α. The collision term for momentum transfer can be evaluated for drifting Maxwell distribution functions, and it is found that

$$\int_{-\infty}^{+\infty} dv_\alpha m v_\alpha \left(\frac{\partial f_\alpha}{\partial t}\right)_{coll} = \sum_\beta m_\alpha n_\alpha \nu_{\alpha\beta}\left(\mu_\alpha - \mu_\beta\right) \tag{8}$$

where μ_α and μ_β are the drift velocities of species α and β. The *charge-charge* collision frequency is given by

$$\nu_{\alpha\beta} = \frac{\left(m_\alpha + m_e\right)}{3\pi^{3/2} m_\alpha^2 m_\beta} \frac{q_\alpha^2 q_\beta^2}{\varepsilon_{si}^2} n_\beta \left(\frac{2\kappa T_\alpha}{m_\alpha} + \frac{2\kappa T_\beta}{m_\beta}\right)^{-3/2} \ln\left(\frac{12\pi\varepsilon_{si}\kappa T}{q_\alpha q_\beta}\sqrt{\frac{\varepsilon_{si}\kappa T}{e^2 n}}\right) \tag{9}$$

where the symbols of α and β denote charge 1 (electron or hole) and charge 2 (hole or electron), respectively. For charge-neutral collisions,

$$v_{q\beta} = \frac{8\pi^{1/2}}{3} \frac{m_\beta}{m_\alpha + m_\beta} n_\beta \sigma^2 \left(\frac{2\kappa T_\alpha}{m_\alpha} + \frac{2\kappa T_\beta}{m_\beta}\right)^{1/2} \tag{10}$$

where σ is the sum of the effective radii of the interacting particles and q denotes the quantum dot which has many properties of natural atoms and is also known as artificial atom.

The optical radiation may also occur via a number of independent competing processes, including the transfer of energy to lattice vibrations (creating one or more phonons) or to another free electron (Auger process). Different types of transition may also take place at surfaces and indirectly via traps or defect centers, which are energy levels associated with impurities or defects associated with grain boundaries, dislocations, or other lattice imperfections that lie within the forbidden band. An impurity or defect state can act as a recombination center if it is capable of trapping both an electron and a hole, thereby increasing their proba-

bility of recombining. The presence of these defects and the high electric field inside the junction result in both a reduction in free carrier density and a reduction of their mobility due to increased scattering of the remaining free carriers with the additional charge centers [29]. Hence, impurity-assisted recombination, which is radiative, should be able to partially characterize the light emission spectrums. More experimental analyses have been made to gain more fundamental insight into the physical nature and origins of the light emission process in avalanching n^+p junctions [30, 31].

Avalanche breakdown has been known to occur along the depletion region, approximated treated as "micro-plasma", and they are visible as shining points. These luminescence micro-plasma spots are connected with defects of the crystal lattice and when they are excited each "micro-plasma" site light up at its own breakdown voltage. It is noted that avalanche process is generally known as an inherently fast process. The modulation speed for the avalanche breakdown mode in the Si-diode LED is also determined by the *RC* time constant. In the PMOSFET device, with the dynamic on-resistance *R* of the "P^+Source/Drain to N-Substrate" junction in the 10^{-2} Ω•cm range and the reverse-bias junction per-unit length capacitance in the range of pF/cm, the *RC* time constant will be in the range of tens of femto-second. Although the capacitance-voltage characteristics of reverse biased p-n junction decreases slowly with reverse-bias voltage V_{sub} as the depletion width W_d increases with reverse-bias voltage V_{sub}, a strong recombination in the avalanche region will induce negative capacitance phenomena that make the capacitance $C_{dep}L_m$ decreases rapidly when the Si-diode LED is fully turned on to avalanche breakdown with hard characteristics (i.e., the multiplication factor is equal to infinity) [32]. Therefore, it is reasonably predicted that the *RC* time will be in the range of tens of pico-second, and such a time delay is capable of producing modulation in excess of 10 GHz. The transit time of the excited carriers is given by

$$\tau_0 = \frac{W_d}{v_s} \tag{11}$$

where W_d is the depletion width of the "P^+Source/Drain to N-Substrate" junction and is the saturated drift velocity of the carriers. Here v_s is also known as the thermal velocity of the carriers, i.e.,

$$v_s \equiv \sqrt{3kT/m} \cong 10^7 \, cm/s \tag{12}$$

Hence, a carrier drifting at v_s ~10^7 cm/s through the length of the depletion region of ~2 μm will set the theoretical limit of light modulation at 20 psec, thus leading to a switching speed ~10 GHz in the Si avalanche electroluminescence devices [33].

To find the relationship between the transit time τ_0 and the reverse current I_{sub}, the characteristics of the p-n junction depletion region is analyzed in detail via the rate of electron-hole generation rate *R*.

http://dx.doi.org/10.5772/58968

$$R + \Delta R = \frac{(n_0 + \Delta n)(p_0 + \Delta p)}{n_0 p_0} R = \frac{n_0 p_0 + p_0 \Delta n + n_0 \Delta p + \Delta n \Delta p}{n_0 p_0} \tag{13}$$

On the other hand, "depletion" is equivalent to saying that most of the space-charge region will be completely depleted of carriers, and the product of excess carrier concentrations, $\Delta n \Delta p$, is a very small term that is negligible. For this case, Eq. (13) reduces to

$$\frac{\Delta R}{R} = \frac{\Delta n}{n_0} + \frac{\Delta p}{p_0} \tag{14}$$

Thus the radiative lifetime of excess carriers is

$$\tau_0 = \frac{\Delta n}{\Delta R} = \frac{1}{R} \frac{n_0 p_0}{n_0 + p_0} \tag{15}$$

Within the depletion region, $n_0 = p_0 = n_i$; therefore, the effective lifetime, also called transit time, within a reverse-biased depletion region is given by [34]

$$\tau_0 = \frac{n_i}{2R} \tag{16}$$

and the reverse current generated in the reverse biased "P^+Source/Drain to N-Substrate" junction can also be expressed as

$$I_{sub} \sim (\tau_0)^{-1} \tag{17}$$

The transit time of excited carriers drifting at approximately the carrier saturation velocity (which is of ~10^7 cm/s) to reach the depletion edge of the p-n junction is defined as the time t required for a filament formation (which could set an upper limit to light modulation speed). On the other hand, a localized fall in the breakdown field and enhancement of fields in the depletion region are analyzed to further understand the transient nature of the filament formation using the 2-D device simulator Silvaco-Atlas. Fig. 7 shows the electric field is of the order of 10^5 V/cm, which implies the transit time is a few pico-seconds and the theoretical limit of light modulation speed is of the order of a few tens of gigahertz. A p-n junction diode device fabricated using a 0.18-μm n-well CMOS process was tested to obtain that light modulation as high as 20 GHz could be observed in a reverse-biased silicon p-n junction operating in avalanche breakdown mode [35]. Accordingly, these signals caused light modulation at 20 GHz frequency is given in Fig. 8.

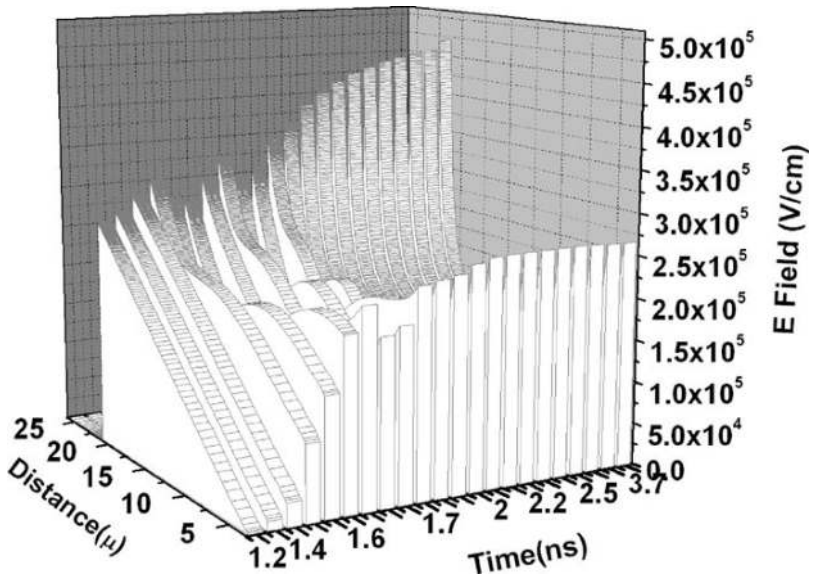

Figure 7. Formation and propagation of an avalanche-breakdown shockwave shows the variation in the electric field (in V/cm) as a function of time and position (After ref. [35]).

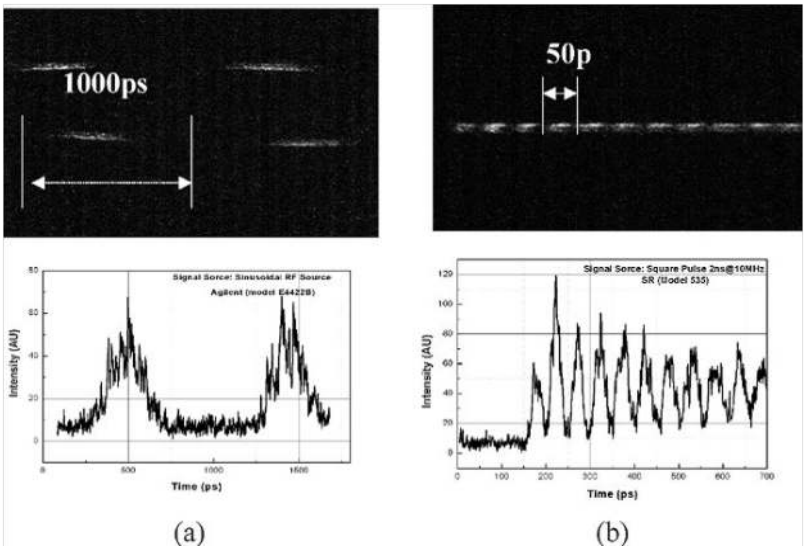

Figure 8. Light emission and intensity measurements of a test structure at: (a) 1 GHz modulation and (b) 20 GHz modulation. The spectrum of the emitted light is distributed between 430–800 nm. (After ref. [35]).

http://dx.doi.org/10.5772/58968

Again, Fig. 2 shows that the proposed Si-PMOSFET device which is fabricated using the standard 3-μm CMOS process can operate as the two-terminal Si-diode LED. In the diode mode, some characteristics of the Si-PMOSFET device are given in [20, 36].

3. Integrated gate-controlled silicon LED

In addition to the study of silicon diode LED in which the light emission is due to the avalanche breakdown of the silicon p-n junction, this section demonstrates the performance of a gate-controlled diode MOS-like multi-terminal device. In contrast to the silicon diode LED (i.e., a two-terminal device), the silicon gate-controlled diode MOS-like LED (i.e., a three-terminal device with an insulated gate on the surface of p-n junction) can use the gate terminal to perform both spatial and light intensity modulation [37–39]. Fig. 9 shows a cross section of the Transconductance Light Emitting Device (TRANSLED) by using a NMOSFET device with a self-aligned poly-silicon MOS gate overlapping an n^+p drain/source junction periphery with a gate oxide thickness of 160 Å working in the accumulation mode, the first gate-controlled three-terminal Si-LED ever reported. Accordingly, the light intensity modulation via the gate voltage is illustrated in Fig. 10, with V_{DD} and R_L kept constant [40].

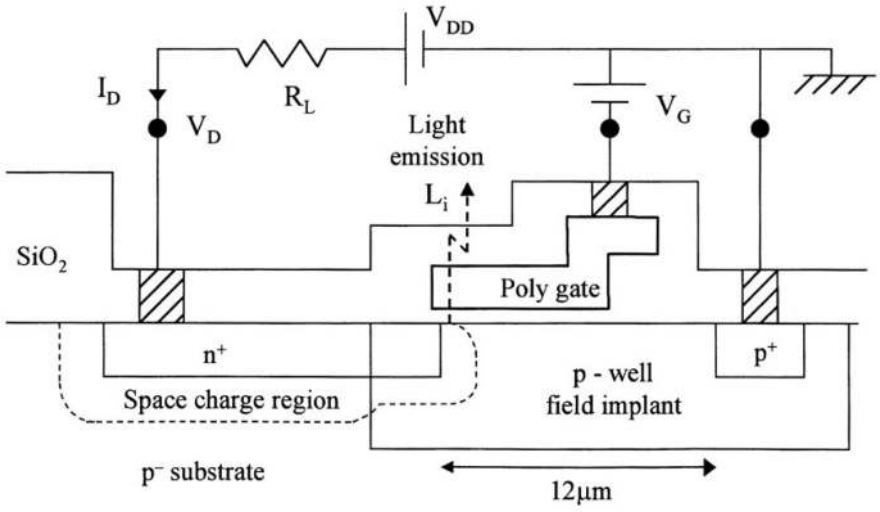

Figure 9. Schematic cross section of the three-terminal gate-controlled TRANSLED, fabricated by standard VLSI technology (After ref. [37]).

Moreover, as shown in Fig. 11, a three-terminal Silicon-PMOSFET-like LED for optical intensity modulation has been discussed in detail based on the concept of p^+n drain/source junction [38, 39].

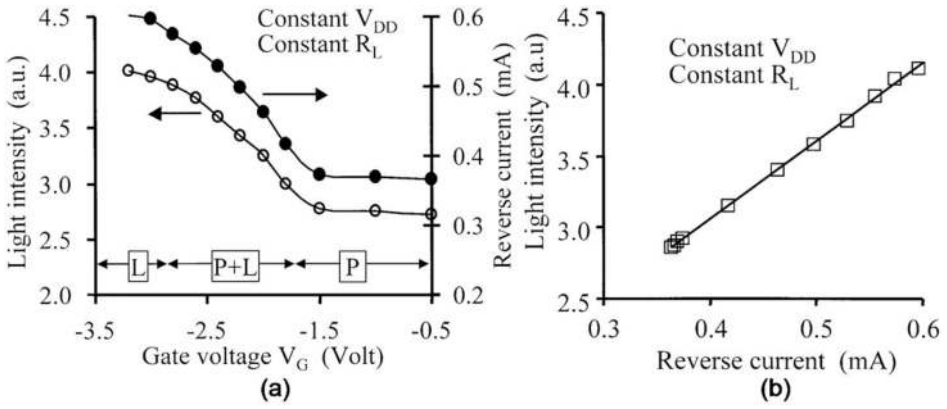

Figure 10. Light emission characteristics of the TRANSLED with constant V_{DD}. (a) Reverse current and overall light intensity, both a s function of V_G. (b) Dependence of the overall light emission on the reverse current (After ref. [40]).

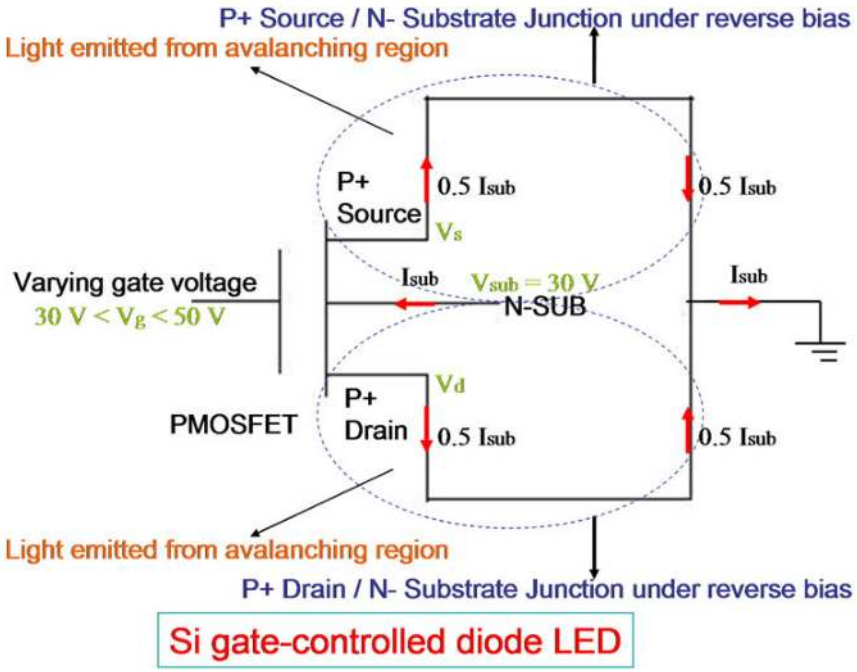

Figure 11. Schematic presentation of the Si-PMOSFET device for the case of Si gate-controlled diode LED (After ref. [41]).

Furthermore, the silicon diode LED (Si-diode LED) is an avalanche-based LED, whereas the silicon gate-controlled diode MOS-like LED (Si gate-controlled diode LED) is a field-emission-

http://dx.doi.org/10.5772/58968

based LED. A discussion of the differences observed between avalanche (Si-diode LED) and field emission LED (Si gate-controlled diode LED) performance is presented in [42], and it is discovered that Si CMOS light sources appears with much higher efficiencies by using a gate terminal to modulate the injection-avalanche p-n junction that emit at 400–900 nm. The enhanced intensity should be mainly due to two possible reasons. One reason is that electron accumulation under the gate oxide with band bending will take place if the positive gate voltage V_g is applied, thus the rate of minority carrier injection into the n-substrate is determined jointly by the P^+S/D to N-Sub bias (i.e., V_{sub} in this measurement because $V_d=V_s=0$ V) and the gate to P^+S/D bias (i.e., V_g in this measurement because $V_d=V_s=0$ V). At a certain PN junction reverse bias, the injection rate could be significantly higher if the gate voltage Vg is applied to make the diode be a gate-diode. This phenomenon is very similar to the carrier barrier lowing effect that occurs in the lateral bipolar transistor [43]. The increased injection rate caused by the positively increased gate voltage V_g may lead to the enhanced emission power observed in the three-terminal device, gate-diode. The other reason why the gated-diode has obviously enhanced emission intensity is that the accumulation of electrons at the surface of the N-Substrate confines the photon emission to the surface of the device, thus reducing the optical absorption by the silicon material itself. In general, an improved quantum efficiency of the gate-controlled diode Si-LED can be obtained, with respect to avalanche Si-LED operating at the same reverse currents (i.e., the avalanching current I_{sub} in this study).

In gate-controlled diode, the breakdown voltage of the p-n junction will be adjustable so that the reverse current I_{sub} flowing through the p-n junction at a fixed reverse-bias voltage is changed. It is observed that the light, which is emitted from the defects located at the p-n junction, depends closely on the reverse current I_{sub}. In regard to the phenomenon of electroluminescence, the relationship between the optical emission power and the reverse current I_{sub} is linear.

Assuming the depletion region of p-n junction to be a micro-plasma, the mechanism can be approximately treated as Bremsstrahlung radiation. Usually, the electron-ion Bremsstrahlung power emitted by the volume of plasma V_p into the solid angle $d\Omega$, and in the wavelength interval $\lambda_s \rightarrow \lambda_s + d\lambda_s$, is

$$P_B d\Omega d\lambda_s = 2.09\times10^{-36} g Z^2 \left(\frac{n_e n_i}{\lambda_s^2\sqrt{T_e}}\right)\exp\left(-\frac{1.24\times10^{-4}}{\lambda_s T_e}\right)V_p\frac{d\Omega}{4\pi}d\lambda_s \tag{18}$$

where Z is the charge on the ion and the Gaunt factor g is temperature and density dependent [44]. After integration, Eq. (18) becomes

$$W_D = \frac{n_e q^2 v}{m_e c\varepsilon_{si}\omega_i^2}\frac{P_i}{A} \tag{19}$$

where W_D is the average power dissipated per unit volume in units of Wm^{-3}, n_e is the carrier concentration in units of m^{-3}, v is the optical frequency, m_e is the effective mass of electron, c is the speed of light, ω_i is the angular velocity, ε_{si} is the dielectric constant of silicon, and $\frac{P_i}{A} = \frac{c\varepsilon_{si}E_{io}^2}{2}$ is the incident power per unit area [45]. In accordance with the relation between hot-carrier effects and electron temperature, the energy distribution function $f(E)$ of photon intensity can be expressed as

$$f(E) = C\exp\left(-\frac{E}{kT_e}\right) \tag{20}$$

where C is a constant, E is the energy of photon, k is the Boltzmann's constant, and T_e is the effective temperature of electron. At the same time, the relative change of electron temperature is given by [46]

$$\frac{\Delta T_e}{T_e} = \frac{\int_0^\tau W_D dt}{1.5\kappa T_e n_e} \tag{21}$$

where τ is the incident pulse duration.

In the case of Si gate-controlled diode LED, higher emission efficiency obtained at lower electric-driving power is attributed to the surface-assisted radiative transitions [39]. Ref. describes the electrical-optical characteristics, and the theoretical calculation and the theoretical calculation and simulation modeling for the topic of modulation speed. The limiting speed of light modulation in reverse-biased silicon p-n junction is analyzed by operating the Si-PMOSFET device in the modes of Si-diode LED and Si gate-controlled diode LED. In Si-diode LED, light emission is due to the avalanche breakdown of p^+source/drain to n-substrate junction and the modulation speed of a few tens of GHz is induced by the intraband transitions of hot carriers and the transit time for sweeping the minority carriers out of the depletion region. In Si gate-controlled diode LED, the p^+source/drain to n-substrate junction breakdown process is triggered by the gate voltage V_g, leading to a localized fall in the breakdown field and enhancement of fields near the p+source/drain to n-substrate junction corner underneath the gate, and the field of the order of 10^6 V/cm is higher than the critical field for avalanche breakdown. Because of the enhancement in electric field, the light modulation speed in Si gate-controlled diode LED will be even much higher [41].

Two additional type of multi-terminal Si-LED's were developed, namely integrated gate controlled (MOS-like structure) array and integrated carrier injection from nearby junction (BJT-like structure) Si-LEDs [47].

http://dx.doi.org/10.5772/58968

4. Light emission from Si-MOSFET's operating in the saturation region

The photo-carrier generation mechanism is fundamentally related to the presence of hot electrons at the drain end of the scaled n-channel MOSFET (N-MOSFET) in which the drain-to-substrate is reverse-biased. Due to the increase in channel current, the drain-substrate p-n junction will reach breakdown, thereby visible light is emitted from the junction region. Furthermore, the conflict between experimentally measured result and theoretically calculated result of the dependence of drain-source current I_{ds} on substrate current I_{sub} shows that there is an secondary impact ionization induced current which is believed to be attributed to the photo-induced process of electron-hole pair generation in the n-type substrate of the N-MOSFET device. This secondarily generated hot-electron (*SGHE*) injection current is also called the minority current observed in the substrate. It is noted that the minority current is the current that is different from the substrate current I_{sub} even if the relationship between the two types of current is almost linear.

Since I_{sub} is mainly due to the mechanism of impact ionization, the relationship between I_{sub} and I_{ds} is given by

$$I_{sub} = I_{ds}\int_0^{L_D} A_i \exp\left[-B_i/\mathrm{E}(y)\right]dy \tag{22}$$

where $\alpha = A_i \exp[-B_i/E(y)]$ is the impact ionization rate, A_i and B_i are the ionization constants and are mainly a function of silicon material parameter itself, and L_D is the length of break-down region near the drain-to-substrate corner. Solving Eq. (22) using a quasi two dimensional (*2-D*) analysis of field $E(y)$, I_{sub} can be derived from I_{ds}

$$I_{sub} = I_{ds}\left(A_i/B_i\right)\left(V_{ds} - \kappa V_{dsat}\right)\exp\left[-L_D B_i/\left(V_{ds} - \kappa V_{dsat}\right)\right] \tag{23}$$

where the peak field E_m is located at $V_{ds} - \kappa V_{dsat} \approx L_D E_m$. $\kappa = 1$ will make sense if L_D is equal to the effective ionization length L_e that is defined as $L_e = \sqrt{(\varepsilon_{si}/\varepsilon_{ox})\, t_{ox} X_j}$ where ε_{si} is the permittivity of silicon, ε_{ox} is the permittivity of SiO_2 (i.e., the insulator layer in N-MOSFET), t_{ox} is the thickness of the SiO_2 layer, and X_j is the junction depth of the drain/source region [48]. In addition to the substrate current, the *SGHE* minority current is given by $I_{SGHE} = C_1((N_C q B_i \lambda_m)/(E_g m_e A_i)) I_{sub}$ where N_c is the number of charged Coulombic centers per volume, λ_m is the mean-free-path, E_g is the band-gap energy, and m_e is the effective mass of electron. As the first two terms are both constants, I_{SGHE} is linear with I_{sub}. Consequently, the relationship between I_{sub} and the optical emission power $P_{optical}$ is linear. It should be noted that the distribution of above-mentioned hot-carrier is defined by the Boltzmann approximation $f(E) = \exp(-E/kT_e)$. Meanwhile, the indirect emission rate of photons in the high-field of is expressed as [49]

$$R_i(h\nu) \infty \int_0^{h\nu - E_g} h\nu f(E)\left[1 - f(E - h\nu)\right]\sqrt{E(h\nu - E_g - E)}dE \tag{24}$$

Substituting $f(E)$ into Eq. (24), it follows as

$$1 - f(E - h\nu) \approx \exp\left[-(E - h\nu)/(kT_e)\right] \tag{25}$$

which implies the Bremsstrahlung radiation because of the quasi-Maxwellian distribution [50]. For the case above, the modulation of light intensity is investigated through the measurement of substrate current in NMOSFET at various gate voltages [51].

5. Realization of first iteration on-chip optical links with Si-Av LEDs, and Si-Ge detectors

Analyses have recently been performed on the viability of integrating Si Av LEDs into standard Si CMOS integrated circuitry or nearest related technology. For this purpose a selection of suitable high speed avalanche diodes based on technology as described above and Si–Ge detector technology as developed by Polleux *et al.* for 650–850 nm detection have been implemented [52]. Several complete optical link structures comprising each of a Si Av LED, an integrated waveguide and a Si–Ge detector were all integrated on the same chip have been all integrated onto the same chip, utilizing a standard Si–Ge RF process that is routinely used for realizing high speed RF integrated circuitry for the cellular phone industry. It was decided to use the Si–Ge RF process as it relates very closely to standard CMOS processes, but it gives an added advantage of realizing Si–Ge detectors in the integrated circuitry, which could then operate at below 1 micron optical wavelength and at very low production factors.

Particularly the realization of suitable optical waveguides were extremely challenging using this technology and approach, and a subsequent thorough investigation were piloted to utilize especially standard "trench and pillar" technology as offered by standard CMOS and RF bipolar processes in order to realize such waveguides. Fig. 12 shows some of the first iteration attempts which includes some details of our first designs. A 0.35 μm RF bipolar process as generally available for the fabrication of RF cell phone components was utilized for the realization process. The process offered pillar/columnar npn epi-layer structure which could be isolated laterally by means of various oxide as TEOS layers.

The analyses show that both silicon nitride and Si oxi-nitride offer good possibilities for transmitting radiation at low loss in the wavelength regime 650–850 nm. Both SiON and Si_3N_5 offer high refractive index of 1.6–1.95 and 2.2–2.4 respectively against a background of available SiO_2 as cladding or background refractive index layers in CMOS silicon [53]. The analytical results by Gorin *et al.* [54] show that a tail-off of absorption from the shorter wavelengths towards the higher wavelengths, via high loss characteristics of 4.3 dB cm^{-1} at 530 nm versus only about 1 dB cm^{-1} at 650 nm and 0.1 dB cm^{-1} loss at 750 nm.

http://dx.doi.org/10.5772/58968

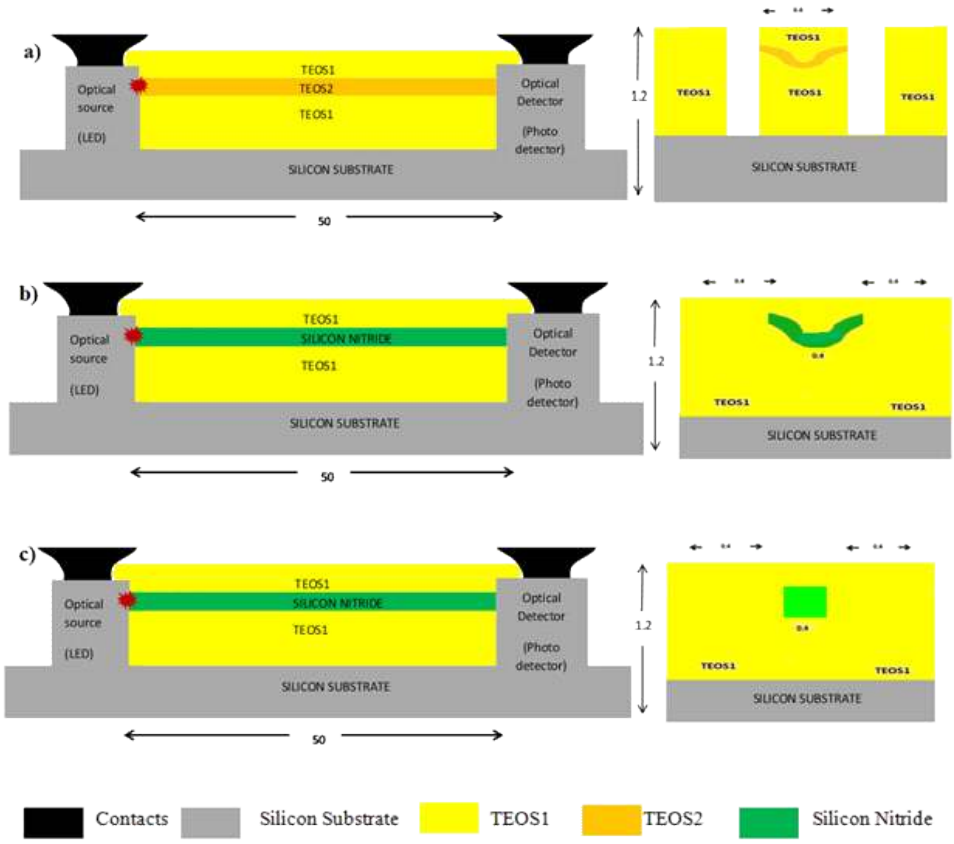

Figure 12. Schematic presentations showing the three basic designs of the waveguides of the optical links as described in this study, using Si Av LED, silicon based waveguides and Si–Ge based detectors. Cross-section layouts of the respective waveguides are given for each design. All dimensions are given in micron and not to scale.

In a first design in Fig.12 (a), the waveguide structure was placed in the outer over layers of the plasma deposit layers. A channel crevice were etched in the TEOS over layers of n=1.46 and then filled with a second TEOS layer. This layer was then densified by a thermal process, increasing its refractive index to about 1.48. A V-shaped cross-section as defined by built-in processing procedures was chosen in order to ensure the highest radiation coupling of the optical source, which was of submicron dimension and spherical in nature, and which was positioned slightly subsurface of the surface of the optical source columnar structure.

In a second design as in Fig 12 (b), an etched crevice of 0.4 micron in the first TEOS layer was filled up with a silicon nitride over layer, followed by further CVD deposited TEOS oxide over-layers. Hence a high refractive index core of “n=2.4” are formed with a surrounding index of “n=1.46”.

In a third design, as in Fig 12 (c), the lateral width of the silicon nitride layer was reduced to about 0.3 micron in order to form a narrow higher index core, which would enable a less multi-mode propagation and lower dispersion of the optical radiation from the source. At shorter wavelengths, silicon nitride and silicon oxi-nitride reveals higher absorption coefficients with good detection efficiency with respect to silicon detectors in a small space volume, while longer wavelengths reveals lower loss transmission but with less efficiency in detection in silicon detectors per unit space volume of silicon.

6. AC analysis for the optical links

The RF coupling between the source and the detectors in the on-chip optical micro-links were analysed with a HP 50GHz vector network analyzer (VNA) series 8510 (50 MHz–40 GHz).

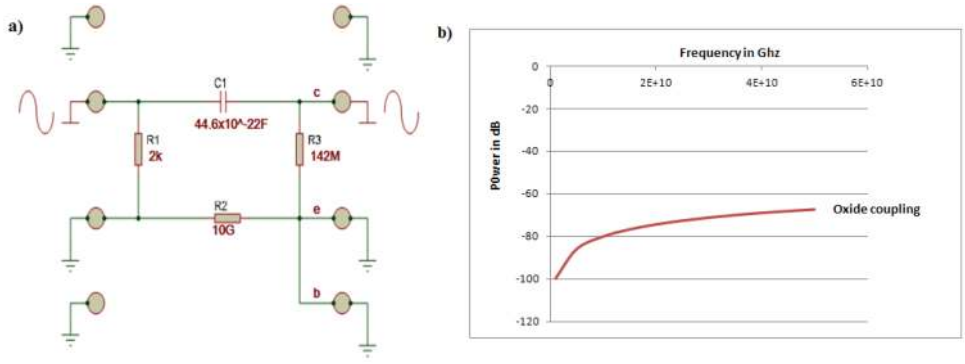

Figure 13. RF Simulation circuitry and plot used for RF coupling analyses of design waveguide-Design1as in Fig. 12 (a).

Simple AC network models of the structure were constructed for each test structure. Fig. 13(a) shows such a circuit for TS1 in simulating the optical link between source and detector. In essence, electrical-to-electrical (E/E) components are microwave two-port circuits and these contained calculated lumped elements for each component as seen by the source signal when placed at the modulation input of the optical source. The value of each lumped element was calculated using known device Design 1 structure dimensions, doping, resistivity and dielectric coefficients of the respective oxide layers. During model circuit simulations, the output power in dB was plotted against the frequency as shown in Fig 13(b).

If such lateral capacitance was indeed present between the detector and the optical source a higher coupling would be observed as modulation frequency is increased. More specifically, an increased RF coupling is observed with increase in frequency, due to the non-linear capacitive coupling.

http://dx.doi.org/10.5772/58968

From our calculations and simulation analyses from the simple waveguide AC network model, the oxide coupling in the structure seems to have a residual-80 dB parasitic coupling when no optical signal was administered at the Si Av LED.

Fig 14 shows some final coupling results for two of the realized optical link structures with regard to utilizing well aligned Si Av LEDs as light emitting sources, an optical waveguide of the type as in Fig. 14(b) and standard Si-Ge detectors as realized by Polleux *et al.* [52].

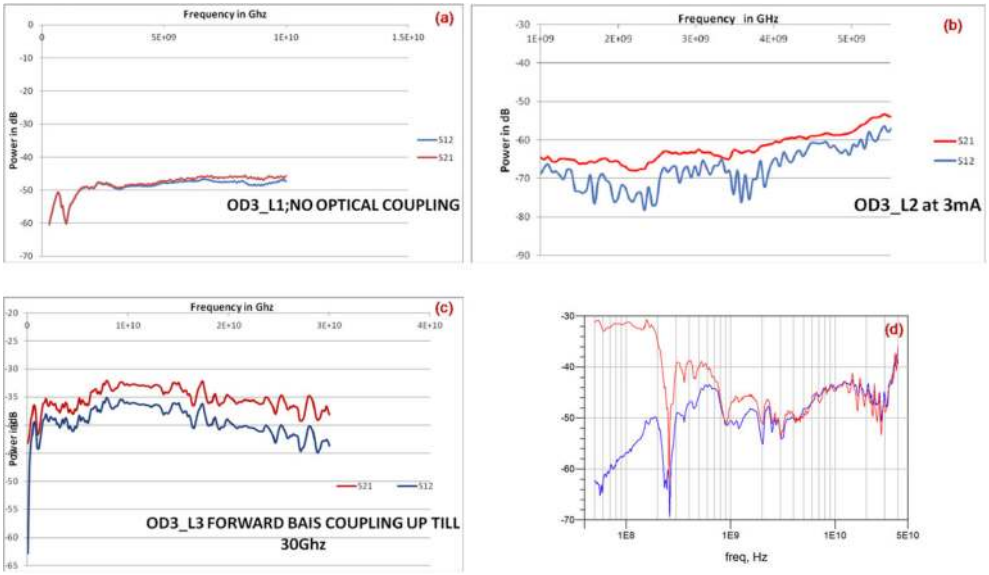

Figure 14. RF coupling results for the realized on-chip micro-optical links. S21 values are indicated as red curves, while S12 are indicated as blue curves. The RF signals were applied at Si Av LED type of devices as elucidated in this chapter (After ref. [53]).

The analyses show clearly higher S21 than S12 for most of the frequency range as investigated. This clearly indicates that some optical propagation did occur along the waveguide. The high S12 value that is observed at higher frequencies is attributed to parasitic conduction along the semi-insulating substrate, when specific capacitance values are analyzed according to the model as in Fig. 12. The capacitive coupling along the oxide layer seems to be minimal and of several orders lower. The fact that higher S21 than S12 is observed up to about 30 GHz and beyond is indicative of the high potential modulation frequencies that can be achieved with Si Av LEDs and even Si-Ge forward bias configurations. Certain design aspects of these structures could still be much improved.

Particularly, further work has been done in utilizing a graded junction concept in order to increase the emission intensity of light as emitting from Si Av LEDs and a high intensity 100 nW 5 GHz Si Av LED using the 0.35 μm micro RF bi-polar process has recently realized [55]. Latest results indicate that due to the enhanced scattering as realized for the highly energized

electrons when they penetrate enhanced scattering zones as offered by higher densities of dopant atoms in traverse regions of the device, increases emission intensities substantially. Currently about 100 fold increase in emission intensities was observed as compared to normal p-n junction configurations. Some tentative results have recently been published in this regard, but substantial refinement still needs to be performed [55]. The concepts as utilized in this device design, relates largely to the carrier recombination and carrier scattering concepts as elucidated in Section 2 of this chapter. It can be anticipated that utilizing this technology in optical link structures, may enhance the preliminary optical link performances as obtained above even more.

7. Conclusion

This chapter discusses a topic of interest, namely the phenomenon of light emission from silicon devices. This topic is important since the search for light emitting devices compatible with the CMOS technology and having an efficiency which is useful for certain applications, is still drawing a lot of attention. Further, this is a potential device that can be fully integrated with any standard CMOS integrated circuitry with no adaptation of the CMOS design and processing procedures [56].

Moreover, light emission from Si NMOSFET operating in the saturation region is reviewed, and it is believed that the light emission is due to the snap-back breakdown that occurs at the high field region near the corner between drain and substrate [57, 58]. The type of light emission is also a sensitive hot-carrier degradation monitor [59].

In applications where high speed data transfer and modulation are required, it is founded that the potential high modulation bandwidths with avalanche-based Si light emitting devices (Si Av LEDs) could be of the order of a few tens of GHz in theory [36, 41]. In order to further analyze the high-speed light modulation in avalanche breakdown mode for Si diodes, Snyman *et al.* utilize the concepts of graded junction, carrier energy and momentum engineering to realize a high intensity 100 nW 5 GHZ Si Av LED using the 0.35 μm micro RF bi-polar process [55], and the silicon light source in combination with silicon-nitride (SiN) based waveguides and high speed silicon-germanium (Si-Ge) based optical detectors [53].

Acknowledgements

The College of Optoelectronic Engineering at the Chongqing University, China, is especially thanked for supporting simulated and experimental analyses as well as facilitating spectroscopic analytic work. I am deeply indebted to Prof. Hongda Chen from the Institute of Semiconductors, Chinese Academy of Sciences, and Prof. Jean-Luc Polleux from the ESIEE Paris, France, and Prof. Lukas Snyman from the TUT in South Africa who provide much-need encouragement while I am finishing the work. Mr. Siyang Liu from the Southeast University,

http://dx.doi.org/10.5772/58968

China, is especially thanked for supporting the earlier electrical simulation and modeling analyses.

Author details

Kaikai Xu[1*], Weifeng Sun[2], Kingsley A. Ogudo[3,4], Lukas W. Snyman[3], Jean-Luc Polleux[4], Qi Yu[1] and Guannpyng Li[5]

*Address all correspondence to: kaikaix@uestc.edu.cn

1 State Key Laboratory of Electronic Thin Films and Integrated Devices, University of Electronic Science and Technology of China, Chengdu, China

2 National ASIC System Engineering Research Center, Southeast University, Nanjing, China

3 Department of Electrical Engineering, Tshwane University of Technology (TUT), Pretoria, South Africa

4 Université Paris-Est, ESYCOM, ESIEE Paris, UPEM, Le Cnam, Cité Descartes, Noisy-Le-Grand-Cedex, France

5 Integrated Nanosystems Research Facility (INRF), University of California, Irvine, California, USA

References

[1] R. Newman, "Visible light from a silicon p-n junction," *Phy. Rev.*, vol. 100, no. 2, pp. 700-704, 1955

[2] A. Chynoweth and K. Mckay, "Photo emission from avalanche breakdown in silicon," *Phys. Rev.*, vol. 102, no. 2, pp. 369-376, 1956

[3] L. Selmi, M. Pavesi, H. Wong, A. Acovic, and E. Sangiorgi, "Monitoring hot-carrier degradation in SOI MOSFET's by hot-carrier luminescence techniques," *IEEE Trans. Electron Devices*, vol. 45, pp. 1135-1139, 1998

[4] D. Miller, "Device requirements for optical interconnects to silicon chips," *Proc. IEEE*, vol. 97, no. 7, pp. 1166-1185, 2009

[5] J. Liu, A. Tolvgard, J. Malmodin, and Z. Lai, "A reliable and environmentally friendly packaging technology-flip-chip joining using anisotropically conductive adhesive," *IEEE Trans. Comp. Packag., Manufact. Technol.*, vol. 22, no. 2, pp. 186-190, 1999

[6] K. Hirschman, L. Tsybeskov, S. Duttagupta, and P. Fauchet, "Silicon-based visible light-emitting devices integrated into microelectronic circuits," *Nature*, vol. 384, no. 6607, pp. 338-341, 1996

[7] G. Reed and A. Kewel, "Erbium-doped silicon and porous silicon for optoelectronics," *Mater. Sci. Eng. B*, vol. 40, no. 2/3, pp. 207-215, 1996

[8] Z. Lu, D. Lockwood, and J. Baribeau, "Quantum confinement and light emission in SiO_2/Si superlattices," *Nature*, vol. 378, no. 6554, pp. 258-260, 1995

[9] T. Komada, J. Kelly, F. Cristiano, A. Nejim, P. Hemment, K. Homewood, R. Gwilliam, J. Mynard, and B. Sealy, "Visible photoluminescence at room temperature from microcrystalline silicon precipitates in SiO_2 formed by ion implantation," *Nucl. Instr. Methods Phys. Res. B*, pp. 387-391, 1995

[10] B. Zheng, J. Michel, F. Ren, and L. Kimerling, D. Jacobson, and J. Poate, "Room-temperature sharp line electroluminescence at λ=1.54 μm from an erbium-doped silicon light-emitting diode," *Appl. Phys. Lett.*, vol. 64, no. 21, pp. 2842-2844, 1994

[11] M. Castagna, S. Coffa, L. Caristia, A. Messina, and C. Bongiorno, "Quantum Dot Materials and Devices for Light Emission in Silicon," in *Proc. 32 nd ESSDERC*, Sep. 24-26, 2002, pp. 439-442

[12] C. Brown, "ST lights up silicon LED for CMOS fab lines," EE Times, La Hulpe, Belgium, Rep., Oct.29, 2002

[13] L. Vescan and T. Stoica, "Room-temperature SiGe light-emitting diodes," *J. Lumin.*, vol. 80, no. 1-4, pp. 485-489, 1999

[14] J. Liu, X. Sun, D. Pan, X. Wang, L. Kimerling, T. Koch, and J. Michel, "Tensile-strained, n-type Ge as a gain medium for monolithic laser integration on Si," *Opt. Exp.*, vol. 15, no. 18, pp. 11272-11277, 2007

[15] J. Liu, X. Sun, L. Kimerling, and J. Michel, "Direct-gap optical gain of Ge on Si at room temperature," *Opt. Lett.*, vol. 34, no.11, pp. 1738-1740, 2009

[16] X. Sun, J. Liu, L. Kimerling, and J. Michel, "Room-temperature direct bandgap electroluminescence from Ge-on-Si light-emitting diodes," *Opt. Lett.*, vol.34, no.8, pp. 1198-1200, 2009

[17] X. Sun, J. Liu, L. Kimerling, and J. Michel, "Direct gap photoluminescence of n-type tensile-strained Ge-on-Si," *Appl. Phys. Lett.*, vol. 95, no. 1, pp. 011911-1–011911-3, 2009

[18] D. Leong, M. Harry, K.J. Reeson, and K.P. Homewod, "A silicon/iron-disilicide light-emitting diode operating at a wavelength of 1.5 μm," *Nature*, vol. 387, no. 6634, pp. 686-688, 1997

[19] I. Pelant and J. Valenta, *Luminescence Spectroscopy of Semiconductors*, Oxford University Press Inc., New York, 2012

http://dx.doi.org/10.5772/58968

[20] K. Xu and G. Li, "Light-emitting device with monolithic integration on bulk silicon in standard complementary metal oxide semiconductor technology," *J. Nanophoton.*, vol. 7, no. 1, 073082, 2013

[21] J. Moll and R. Overstraeten "Charge multiplication in silicon p-n junctions," *Solid State Electron.*, vol. 6, no. 2, pp. 147-157, 1963

[22] N. Akil, S. Kerns, D. Kerns, A. Hoffmann, and J. Charles, "A multimechanism model for photon generation by silicon junctions in avalanche breakdown," *IEEE Trans. Electron, Dev.*, vol. 46, no. 5, pp. 1022-1028, 1999

[23] A. Lacaita, F. Zappa, S. Bigliasrdi, and M. Manfredi, "On the bremsstrahlung origin of hot-carrier-induced photons in silicon devices," *IEEE Trans. Electron. Dev.*, vol. 40, no. 3, pp. 577-582, 1993

[24] J. Bude, N. Sano, and A. Yoshi, "Hot-carrier luminescence in silicon," *Phys. Rev. B*, vol. 45, no. 11, pp. 5848-5856, 1992

[25] S. Glenzer, G. Gregori, F. Rogers, D. Froula, S. Pollaine, R. Wallace, and O. Landen, "X-ray scattering from solid density plasmas," *Phys. Plasmas*, vol. 10, no. 6, pp. 2433-2441, 2003

[26] T. Brandes, "Coherent and collective quantum optical effects in mesoscopic systems," *Phys. Rep.*, vol. 408, iss. 5-6, pp. 315-474, 2005

[27] W. Itano and D. Wineland, "Laser cooling of ions stored in harmonic and penning traps," *Phys. Rev. A*, vol. 25, no. 1, pp. 35-54, 1982

[28] H. Zohm, "Physics of "hot" plasma," *Let. Notes Phys.*, 670, pp. 75-93, 2005

[29] F. McLean, J. McGarrity, C. Scozzie, C. Tipton, and W. Delancey, "Analysis of neutron damage in high-temperature silicon carbide JFETs," *IEEE Trans. Nucl. Sci.*, vol. 41, no. 6, pp. 1884-1894, 1994

[30] L. Snyman, H. Aharoni, M. du Plessis, and R. Gouws, "Increased efficiency of silicon light-emitting diodes in a standard 1.2-μm silicon complementary metal oxide semiconductor technology," *Opt. Eng.*, vol. 37, no. 7, pp. 2133-2141, 1998

[31] L. Snyman, M. du Plessis, E. Seevinck, and H. Aharoni, "An efficient low voltage, high frequency silicon CMOS light emitting device and electro-optical interface," *IEEE Electron Device Lett..*, vol. 20, no. 12, pp. 614-617, 1999

[32] C. Wang, C. Zhu, G. Zhang, J. Shen, and L. Li, "Accurate electrical characterization of forward AC behavior of real semiconductor diode: giant negative capacitance and nonlinear interfacial layer," *IEEE Trans. Electron Devices*, vol. 50, no. 4, pp. 1145-1148, 2003

[33] F. Stellari, F. Zappa, S. Cova, C. Porta, and J. Tsang, "High-speed CMOS circuit testing by 50 ps time-resolved luminescence measurements," *IEEE Trans. Electron Devices*, vol. 48, no. 12, pp. 2830-2835, 2003

[34] D. Sandiford, "Carrier lifetime in semiconductors for transient conditions," *Phys. Rev.*, vol. 105, no. 2, p. 524, 1957

[35] A. Chatterjee, B. Bhuva, and R. Schrimpf, "High-speed light modulation in avalanche breakdown mode for Si diodes," *IEEE Electron Device Lett.*, vol. 25, no. 9, pp. 628-630, 2004

[36] K. Xu, "On the design and optimization of three-terminal light-emitting device in silicon CMOS technology," *IEEE J. Sel. Topics Quantum Electron.*, vol. 20, no. 4, 8201208, July/Aug, 2014

[37] M. du Plessis, H. Aharoni, and L. Snyman, "A silicon transconductance light emitting device (TRANSLED)," *Sens. Actuators, A.*, vol. 80, no. 3, pp. 242-248, 2000

[38] K. Xu and G. Li, "A three terminal silicon-PMOSFET like light emitting device (LED) for optical intensity modulation," *IEEE Photonics J.*, vol. 4, no. 6, pp. 2159-2168, 2012

[39] K. Xu, "Current-voltage characteristics and increase in the quantum efficiency of three-terminal gate and avalanche-based silicon LEDs," *Appl. Opt.*, vol. 52, no. 27, pp. 6669-6675, 2013

[40] M. du Plessis, H. Aharoni, and L. Snyman, "Silicon LED's fabricated in standard VLSI technology as components for all silicon monolithic integrated optoelectronic systems," *IEEE J. Sel. Top. Quantum Electron.*, vol. 8, no. 6, pp. 1412-1419, 2002

[41] K. Xu, "Electro-optical modulation processes in Si-PMOSFET LEDs operating in the avalanche light emission mode," *IEEE Trans. Electron Devices*, vol. 61, no. 6, pp. 2085-2092, 2014

[42] K. Xu and G. Li, "A novel way to improve the quantum efficiency of silicon light-emitting diode in a standard silicon complementary metal-oxide-semiconductor technology," *J. Appl. Phys.*, vol. 113, no. 10, 103106, 2013

[43] Z. Yan, M. Deen, and D. Malhi, "Gate-controlled lateral PNP BJT: Characteristics, Modeling and Circuit Applications," *IEEE Trans. Electron. Devices*, vol.44, no.1, pp. 118-128, 1997

[44] C. Fortmann, A. Wierling, and G. Ropke, "Influence of local-field corrections on Thomson scattering in collision-dominated two-component plasma," *Phys. Rev. E*, 81, 026405, 2010

[45] E. Gusakov, A. Gurchenko, A. Altukhov, A. Stepanov, L. Esipov, M. Kantor, and D. Kouprienko, "Investigation of ETG mode-scale component of tokamak plasma turbulence by correlative enhanced scattering diagnostics," *Plasma Phys. Control. Fusion* 48, 371-376 (2006)

[46] B. Kronast, H. Rohr, E. Glock, H. Zwicker, and E. Funfer, "Measurements of the ion and electron temperature in a theta-pinch plasma by forward scattering," *Phys. Rev. Lett.* 16, 1082-1085 (1966)

[47] M. du Plessis, H. Aharoni, and L. Snyman, "Two-and multi-terminal silicon light emitting devices in standard CMOS/BiCMOS IC technology," *Physics Status Solidi A*, vol. 201, no. 10, pp. 2225-2233, 2004

[48] N. Akil, S. Kerns, D. Kerns, A. Hoffmann, and J. Charles, "A multi-mechanism model for photon generation by silicon junction in avalanche breakdown," *IEEE Trans. Electron Devices*, vol. 46, no. 5, pp. 1022-1028, 1999

[49] S. Yamada and M. Kitao, "Recombination radiation as possible mechanism of light emission from reverse-biased p-n junctions under breakdown condition," *Jpn. J. Appl. Phys.*, vol. 32, no. 10, pp. 4555-4559, 1993

[50] H. Elghazi, A. Jorio, and I. Zorkani, "Analysis of silicon light emission under breakdown condition using an indirect intraband model," *Opt. Commun.*, vol. 281, iss. 12, pp. 3320-3323, 2008

[51] M. Gurfinkel, M. Borenshtein, A. Margulis, S. Sade, Y. Fefer, Y. Weizman, and Y. Shapira, "Study of hot-carrier-induced photon emission from 90 nm Si MOSFETs," *Appl. Surf. Sci.*, vol.248, issu. 62-65, 2005

[52] J. Polleux, F. Moutier, A. Billabert, C. Rumelhard, E. Sönmez, H. Schumacher, "A Strained SiGe layer Heterojunction Bipolar Phototransistor for Short-Range Opto-Microwave Applications", in *IEEE International Topical Meeting on Microwave Photonics*, MWP2003, Budapest, Hungary, Sep. 2003

[53] K. Ogudo, L. Snyman, J. Polleux, C. Viana, Z. Tegegne, and D. Schmieder, "Toward 10-40 GHz on-chip micro-optical links with all integrated Si Av LED optical sources, Si N based waveguides and Si-Ge detector technology," *Proc. SPIE*, vol. 8991, 899108-1–16, 2014

[54] A. Gorin, A. Jaouad, E. Grondin, V. Aimez, and P. Charette, "Fabrication of silicon nitride waveguides for visible-light using PECVD: a study of the effect of plasma frequency on optical properties," *Opt. Exp.*, vol. 16, iss. 18, pp. 13509-13516, 2008

[55] L. Snyman, J. Polleux, K. Ogudo, C. Viana, and S. Wahl, "High intensity 100 nW 5 GHz silicon avalanche LED utilizing carrier energy and momentum engineering," *Proc. SPIE*, vol. 8990, 89900L-1–12, 2014

[56] K. Xu, "Electric field modulation of light emission in silicon gated diodes," Ph.D. dissertation, University of California, Irvine, CA, July 2014

[57] G. Teh, W. Chim, Y. Swee, and Y. Co, "Spectroscopic photon emission measurements of n-channel MOSFETs biased into snapback breakdown using a continuous-pulsing transmission line technique," *Semicond. Sci. Technol.*, vol. 12, no. 6, pp. 662-671, 1997

[58] L. Selmi, M. Pavesi, H. Wong, and E. Sangiorgi, "Monitoring hot-carrier degradation in SOI MOSFET's by hot-carrier luminescence techniques," *IEEE Trans. Electron Devices*, vol. 45, no. 5, pp. 1135-1239, 1998

[59] K. Xu, "Hot carrier luminescence in silicon metal oxide semiconductor field effect transistor," in Advances in Optoelectronics Research, Nova Science Publisher Inc., New York, pp. 1-28, 2014